

Magnetic ordering in (110) Eu films in an applied magnetic field

S. Soriano^{1,2}, C. Dufour^{1,a}, K. Dumesnil¹, and Ph. Mangin⁴

¹ Laboratoire de Physique des Matériaux, Université H. Poincaré-Nancy I, BP 239, 54506 Vandoeuvre-les-Nancy Cedex, France

² Universidade Federal do Rio de Janeiro, Instituto de Física, 21945-970, Rio de Janeiro-RJ, Brazil

³ LLB, CEA Saclay, 91191 Gif-sur-Yvette, France

Received 22 October 2007 / Received in final form 10 April 2008

Published online 10 July 2008 – © EDP Sciences, Società Italiana di Fisica, Springer-Verlag 2008

Abstract. Below its ordering temperature ($T_N = 90$ K), bulk bcc Eu has a helical magnetic state with propagation vectors along the three equivalent $\langle 100 \rangle$ directions. In contrast, epitaxial (110)Eu films exhibit a unique magnetic ordering : the domain with a magnetic helix propagating along the in-plane [001] direction vanishes on cooling, at the expense of other domains with helices propagating along [100] and [010]. This paper is devoted to the study of the stability of the magnetic domains in an external magnetic field using neutron scattering experiments and macroscopic magnetization measurements. The helix propagating along the [001] direction can be restored by the application of an external field along this direction. On the contrary, when a magnetic field is applied along an intermediate direction, specifically $[\bar{1}10]$, the domain with a helix propagating along [001] is suppressed. Both effects depend on the film thickness. They are explained if one considers that, because of the low magnetic anisotropy of Eu, a helix with a propagation vector parallel to (or close to) the applied magnetic field is energetically more favourable than cycloidal structures with unchanged propagation vectors. Finally, the amplitudes of the propagation vectors and their directions (that are modified in films compared to bulk) do not vary under magnetic field.

PACS. 75.25.+z Spin arrangements in magnetically ordered materials – 75.70.Ak Magnetic properties of monolayers and thin films – 68.55.-a Thin film structure and morphology – 61.12.Ex Neutron scattering

1 Introduction

Bulk rare earth metals exhibit complex magnetic phase diagrams resulting from the competition between exchange energy, magnetic anisotropy and magnetostriction [1]. Rare earth epitaxial films are ideal candidates for fundamental studies of the link between structural and magnetic properties. In fact, in these films, both the lattice clamping to the substrate and the pseudomorphic strains are known to induce modifications of the magnetic properties [2–8].

Europium is an atypical light rare earth that is divalent and has a half-filled $4f$ shell. These characteristics lead to physical and chemical properties that significantly differ from most other rare earths [9]: for example, Eu has a bcc crystal structure, low melting point, large atomic radii, large thermal expansion coefficient, etc...

In its bulk form, Eu undergoes a first order magnetic transition [10] to a helical state below the Néel temperature T_N close to 90 K [11]. The propagation vectors of the helices are along the $\langle 100 \rangle$ directions with a turn angle that slightly decreases from 51.4° at the transition temperature to 50° at 4.2 K. The magnetic moments lie in $\{100\}$ planes perpendicular to the propagation wave vectors and are aligned ferromagnetically within these planes.

Six magnetic domains are thus present; the corresponding propagation vectors are: $\pm\kappa_1 = (\pm\tau\ 0\ 0)$; $\pm\kappa_2 = (0 \pm\tau, 0)$; $\pm\kappa_3 = (0 \pm\tau, \tau)$. τ is the magnitude of the wave vector of the periodic magnetic structure ($\tau = 0.3926\text{\AA}^{-1}$). We adopt a simplified notation D_i representing domains with propagation vectors $\pm\kappa_i$ (with opposite helicities). D_1 , D_2 and D_3 develop with a-priori equal proportions. The magnetic transition is accompanied by an abrupt tetragonal distortion (+0.09% along an axis and -0.044% along the two other ones) [12].

The application of a magnetic field along one of the $\langle 100 \rangle$ cubic directions stabilizes the propagation of a magnetic helix along this direction [13]. Actually, because the magnetic anisotropy of Eu is very small, it is therefore energetically more favorable to change the helix propagation vectors towards the field direction rather than for the helix to distort in its plane, leaving the propagation vectors fixed and forming cycloidal structures. When increasing magnetic field, a conical ordering of the moment is expected, with an apex angle of the cone becoming always smaller, leading finally to a ferromagnetic arrangement of the moments. When a magnetic field is applied along [001], at 4.2 K, D_3 increases gradually between 0.5 and 2 T at the expense of D_1 and D_2 [13]; because of hysteretic effects, D_1 and D_2 reappear in zero field only after heating the

^a e-mail: dufour@lpm.u-nancy.fr

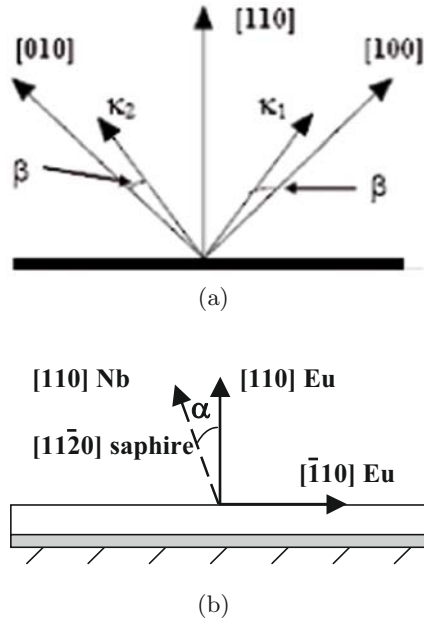


Fig. 1. (a) Sketch of the rotation angle β between the magnetic propagation vectors and the crystal axes in (110)Eu films. (b) Sketch of the tilt angle α between the [110] growth direction of Eu and the [1120] direction in the sapphire substrate in (110)Eu films.

sample to 35 K. There is no rotation of the propagation vectors towards the field direction. On the contrary, when a magnetic field is applied along the $[\bar{1}10]$ direction (not a magnetic propagation direction), the helix propagating along [001] disappears above 0.7 T whereas the proportions of the domains with helices propagating along [100] and [010] decreases under a much higher field [13]. Due to the large absorption of neutron beam by Eu, a refinement of the magnetic structure of bulk Eu in a $[\bar{1}10]$ magnetic field has not been successful.

Single crystal (110) Eu films have been prepared only recently by Molecular Beam Epitaxy (MBE) [14]. A unique magnetic structure has been reported under zero magnetic field [15]: when decreasing temperature, D_1 and D_2 grow at the expense of D_3 (the domain with a helix propagating along the in-plane [001] direction). In addition, the propagation vectors in D_1 and D_2 continuously rotate towards the [110] growth direction with decreasing temperature. The angle of rotation β (Fig. 1a) is temperature dependent. These behaviors are correlated to the onset of shear strains below T_{cl} , the temperature below which the film's lattice is constrained to follow the thermal expansion of the substrate [16]. In fact, the lattice strains introduce a new magnetoelastic term in the total energy of the system that favors the change of the moment directions for D_1 and D_2 . Consequently, the magnetoelastic contribution induces a rotation of the magnetic propagation direction, provided this direction remains perpendicular to the plane containing the magnetic moments [17]. Tilting the magnetic propagation vectors κ_1 and κ_2 reduces either the exchange or magnetoelastic energies of

D_1 and D_2 . D_3 likely vanishes below a temperature T_d , when its energy cost becomes too high. All these effects are thickness dependant (Tab. 1), since the different contribution to the total energy are weighted by the thickness of the Eu film and of the non-magnetic buffer (responsible for the clamping effect).

This paper reports results of a combined neutron scattering and macroscopic magnetization measurements study of the stability of the magnetic domains in (110) Eu films under magnetic field. The magnetic field was applied along two directions of the (110) plane: (i) the [001] direction, parallel to a magnetic propagation wave vector; and (ii) the $[\bar{1}10]$ direction located at 45° from the [100] and [010] propagation vectors.

The paper is organized as follows: the second section is devoted to the films growth and atomic structure characterization. The main results involving the response of the magnetic structure to the applied field are presented in the third section.

2 Films growth and atomic structure characterization

The Eu films were fabricated by MBE, following a specific process developed to get high quality single crystals on $[11\bar{2}0]$ sapphire substrates [14]. A 50 nm (110)Nb buffer is first deposited at 800 °C. The Nb surface is reconstructed due to the presence of chemisorbed oxygen [18] and favors the stabilization of a hexagonal Eu surface, the relaxation of which gives rise to a multi-domain bcc Eu film. However, if an additional 15 nm layer of (110)Nb is deposited at 150 °C on the initial Nb buffer layer, a non-reconstructed (110)Nb surface forms that allows growth of single crystal (110)Eu. Eu films were grown with thickness ranging between 37.5 nm and 750 nm. The samples were covered with a 100 nm thick yttrium cap layer to prevent the highly reactive Eu deposit to oxidize.

The crystal quality of the films was checked using X-ray scattering. We find the crystalline coherence length along the growth direction increases from 24 nm to 60 nm when the films thickness increases from 37.5 nm to 750 nm and the mosaicity decreases from 1.07° to 0.18° in the same thickness range. Table 1 presents a list of the films and their main structural characteristics. In some samples, the Eu growth direction is slightly tilted, probably due to a substrate miscut, as designated by the angle α sketched in Figure 1b. The values of the angle α determined for the whole set of samples from X-ray diffraction are also listed in Table 1.

In-plane and out-of-plane lattice constants of Eu films were measured at 300 K by X-ray scattering and as a function of temperature down to 10 K using neutron scattering [17]. At low temperature, the Eu is no longer cubic, but is distorted with the in-plane $a_{[\bar{1}10]}$ and $a_{[002]}$ lattice constants larger than the $a_{[110]}$ lattice constant along the growth-axis. In fact, below a clamping temperature T_{cl} , $a_{[\bar{1}10]}$ and $a_{[002]}$ are clamped to the underlying Nb buffer layer. They leave the thermal reduction observed in bulk Eu and remain almost constant down to 10 K.

Table 1. List of the samples, thicknesses, structural coherence length, mosaïcity and tilt angle α determined from X-ray diffraction, relative proportions P_i of the magnetic domains at 10 K, angle β and temperature of disappearance of the domain D_3 under zero magnetic field determined from neutron and magnetic X-ray diffraction.

sample	thickness (nm)	Coh. length (± 2 nm)	Mosaï- -city ($\pm 0.02^\circ$)	Tilt $\alpha \pm 0.05$ ($^\circ$)	P_1 at 10 K (%)	P_2 at 10 K (%)	P_3 at 10 K (%)	β at 10 K ($^\circ$)	T_d (K)
Bulk	/	/	/	0	33.33	33.33	33.33	0	0
Film A	37.5	24	1.07	0.55	52	48	0	7.1	/
Film B	75	39	0.72	0	39	61	0	4.8	55
Film C	80	39	0.76	1.32	86	14	0	5.17	/
Film D	150	50	0.73	1.88	92	8	0	5.3	50
Film E	375	51	0.58	0	45	55	0	3.8	42
Film F	375	59	0.25	1.4	97	3	0	3.5	45
FilmG	750	60	0.18	0	57	43	0	1.87	37

However, the clamping of the in-plane lattice parameters does not affect the bulk-like temperature dependence of the perpendicular lattice parameter, because the Poisson coefficient of Eu is small (0.15). This clamping effect leads to a negative shear strain ε_{xy} of the same order of magnitude as the one measured in the (110)REFe₂ (RE= rare earth) [19] and the (110)Cr [20] epitaxial films. The absolute value of shear strain increases when the temperature decreases. The well-defined clamping temperature strongly depends on the Eu thickness. Consequently, the shear strain is also thickness dependent: its magnitude increases when the film thickness decreases. At 10 K, ε_{xy} varies between -0.15% for a 750 nm thick Eu film and -0.5% for a 37.5 nm one (Tab. 1). The origin of the clamping temperature and its systematic dependence upon Eu thickness remains to be clarified, though it likely is related to the thermal mobility of misfit dislocations.

3 Magnetic ordering under magnetic field in (110)Eu films

3.1 Experimental details

The macroscopic magnetization measurements were performed using a Quantum Design SQUID magnetometer.

Neutron scattering experiments were performed at the Laboratoire Léon Brillouin in Saclay (France) on the 4F2 triple axis instrument with the crystal analyzer set for zero-energy transfer (to improve the signal to background ratio). The neutron wavelength was 2.36 Å. The collimation was 40' before and after the sample, leading to an instrumental resolution of 0.016 Å⁻¹. The sample was placed in a cryomagnet with vertical field. The measurements were performed in the temperature range 10 K–300 K and in the field range 0 T–5 T.

The distribution of coherent nuclear and magnetic intensities for bulk bcc Eu is presented in Figure 2. Three pairs of magnetic satellites are located around each (hkl) nuclear peak at $(h \pm \tau, k, l)$, $(h, k \pm \tau, l)$ and $(h, k, l \pm \tau)$. In order to simplify the notation, around a given nuclear peak, the magnetic peaks associated respectively to the

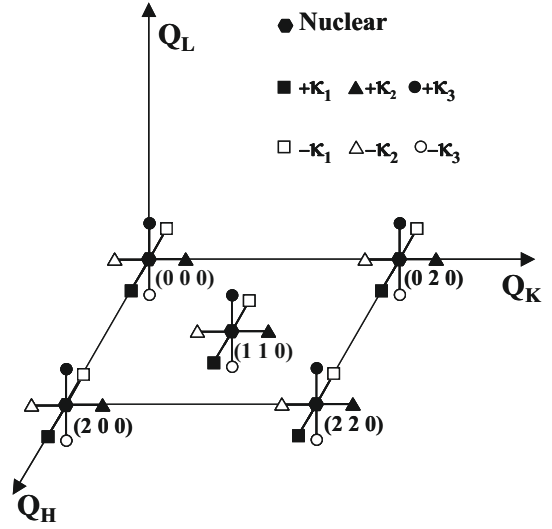


Fig. 2. Reciprocal lattice of magnetic bcc Eu: nuclear scattering peaks (diamonds), magnetic scattering peaks corresponding to the helices with propagation vectors along $[100]$ (squares), $[010]$ (triangles) and $[001]$ (circles).

D_1 , D_2 and D_3 domains are labeled using the corresponding propagation vectors $\pm\kappa_1$, $\pm\kappa_2$ and $\pm\kappa_3$.

3.2 Magnetic ordering for a magnetic field applied along the [001] direction

Before to present data under magnetic field, let's underline a zero field result: as a consequence of the tilt (α angle) of the Eu growth direction (paragraph 2), the $[100]$ and $[010]$ cubic axis are no longer equivalent. So, the proportions of D_1 and D_2 in zero field depend on this tilt angle. Their values P_i at 10 K are presented in Table 1. At low temperature, P_3 is always equal to zero. When the tilt angle α is smaller than 1° , P_1 is close to P_2 ; on the contrary, when α is larger than 1° , P_1 is larger than P_2 ($P_1 = 100\%$, 97% , 86%).

In this section, we report results obtained for a magnetic field applied along the $[001]$ direction, parallel to

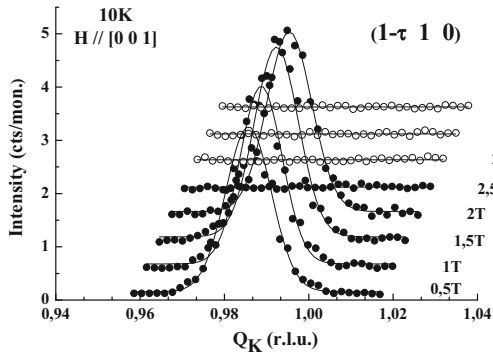


Fig. 3. Neutron diffraction spectra collected for the film F along the b^* direction. Evolution of the $-\kappa_1$ magnetic satellite (around the $(1 - \tau, 1, 0)$ reflection) at 10 K as a function of the magnetic field applied along the $[001]$ direction. Filled and empty symbols correspond respectively to the increase and the decrease of the magnetic field. The curves have been shifted vertically to improve clarity.

the magnetic propagation vector in D_3 and located in the sample plane. Detailed data are first shown for the 375 nm thick (110) Eu film with a tilt angle larger than 1° (sample F, paragraph 3.2.1); then the influence of film thickness on the magnetic structure is presented (paragraph 3.2.2).

3.2.1 Magnetic ordering in a 375 nm thick (110) Eu film

a) Neutron diffraction under magnetic field.

The positions and the intensities of the magnetic satellites observed by neutron diffraction were recorded as a function of magnetic field. The positions of the satellites do not vary with magnetic field suggesting that the turn angle of the helix and the direction of propagation are not affected by the magnetic field. On the contrary, the intensities (and thus the values of P_1 , P_2 and P_3) strongly depend on the magnetic field.

When the film is first cooled to low temperature in zero field (ZFC process), D_1 is mainly present: a single pair of magnetic satellites, labeled κ_1 and $-\kappa_1$ are observed around each nuclear peak and $P_1 = 97\%$, (Tab. 1). Both satellites disappeared in a range between 2 T and 2.5 T. This process is irreversible, i.e. the κ_1 and $-\kappa_1$ satellites remain absent even if the field is reduced to zero. As an illustration, Figure 3 presents the $-\kappa_1$ satellite as a function of field. After reducing the field to zero, a detailed analysis of the reciprocal space permits to evidence that only D_2 is present. To restore D_1 , one needs to warm the sample up to 300 K and then to cool it down again. Thus, at 10 K and zero field, P_3 is always equal to zero but $P_1 \gg P_2$ or $P_2 \gg P_1$ depending on the magnetic history of the sample.

Figures 4a and 4b show the variation of the intensities of the $-\kappa_2$ and κ_3 satellites at 10 K as a function of magnetic field, starting from a magnetic configuration with $P_3 = 0$ and $P_2 \gg P_1$. The $-\kappa_2$ satellite suddenly disappeared for a critical field $H_a = 2.4$ T, while the κ_3 satellite simultaneously appeared. The effect was hysteretic: when

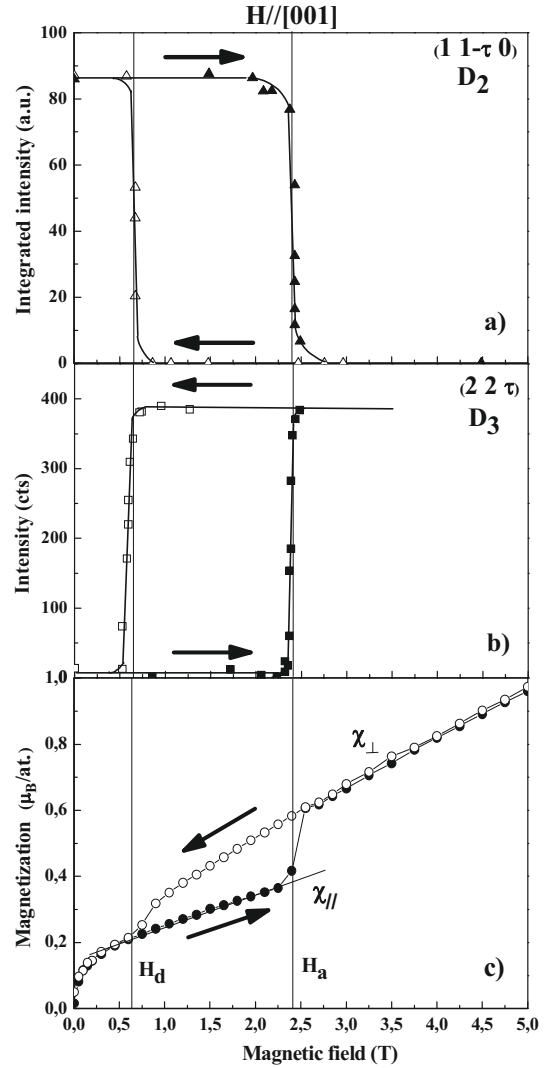


Fig. 4. Intensities of the $(1, 1 - \tau, 0)$ (a) and $(2, 2, \tau)$ (b) magnetic satellites and macroscopic magnetization (c) as a function of the magnetic field applied along the $[001]$ direction at 10 K for sample F. Filled and empty symbols correspond respectively to the increase and the decrease of the magnetic field.

decreasing the field, the κ_3 satellite vanished for a critical field $H_d = 0,7$ T and D_2 was simultaneously restored. Note that the variation of the intensities of the $-\kappa_2$ and κ_3 magnetic satellites at H_a and H_d are abrupt. Restoration of D_3 at H_a and its disappearance at H_d were also observed starting from a magnetic configuration with $P_3 = 0$ and $P_1 \gg P_2$.

Consequently, as in bulk Eu, the magnetic field applied along the $[001]$ magnetic propagation vectors tends to favor the corresponding D_3 domain at the expense of the other domains. However, the (110)Eu films behavior is notably different from the bulk for two reasons:

- (i) the value of the magnetic field necessary to suppress D_1 and/or D_2 is more than twice that for bulk Eu (2.4 T vs. 1 T [13]).

- (ii) in bulk, the magnetic ordering induced under magnetic field (favoring D_3 only) is irreversible. To restore the initial magnetic ordering (equal size magnetic domains), the sample must be warmed at 35 K. In the film F, the vanishing, under magnetic field, of the domain stabilized by a ZFC process (D_1) is also irreversible. However, when cycling the magnetic field at low temperature, D_3 and D_2 are successively stabilized.

Both points (i) and (ii) are consistent with the fact that D_3 is not favored compared to D_1 and D_2 in (110)Eu films in zero field (lattice strain effect).

The small decrease of intensity associated to the D_2 domain for magnetic fields slightly smaller than H_a can be attributed to a slight distortion of the helix. This assumption is in agreement with the small value of the magnetic susceptibility for an helical order with small anisotropy when the magnetic field is applied in the plane of the helix [21,22].

b) Macroscopic magnetization as a function of field and temperature

At 10 K, the first magnetization curve measured for a magnetic field along [001] after zero field-cooling exhibits a rather small slope (between 0.2 T and H_a), followed by an abrupt and significant increase when the field becomes larger than H_a (Fig. 4c). Above H_a , the slope of the magnetization curve is similar to bulk Eu. As in bulk Eu [7,8], there is no sign of any saturation for large magnetic fields. When decreasing magnetic field, a decrease of the magnetization is observed at $H_d = 0.7$ T (along the applied field direction).

These jumps of magnetization can be correlated to the relative variation of the proportion of the magnetic domains observed during neutron experiments (Figs. 4a and 4b). The D_1 and/or D_2 domain configuration occurs for $H < H_a$ when increasing field and for $H < H_d$ when decreasing field. The single D_3 domain configuration is observed for $H > H_a$ when increasing field, and for $H > H_d$ when decreasing field. The formation of D_3 leads to the increase of the net magnetisation along the [001] direction at H_a and its vanishing leads to the decrease of the magnetisation at H_d .

These jumps of magnetization on the $M(H)$ curves are clearly visible for temperatures below 45 K. However, when increasing temperature from 10 K to 45 K, they are shifted towards smaller values of the magnetic field ($H_a = 1.4$ T at 40 K). On the contrary, in the temperature range where the three magnetic domains are present for $H = 0$ ($T > T_d = 45$ K), no jump of the magnetization is observed and the behavior of the film is close to that of bulk (without any jump, nor hysteretic effect).

The origin of the high susceptibility observed at low field in Figure 4c is still under investigation. From neutron diffraction, it is not due to the occurrence of a pollution (oxide...) but perhaps to a magnetic re-arrangement of the helix of the D_1 and/or D_2 domain under field. Our present aim being to study the new features, compared to

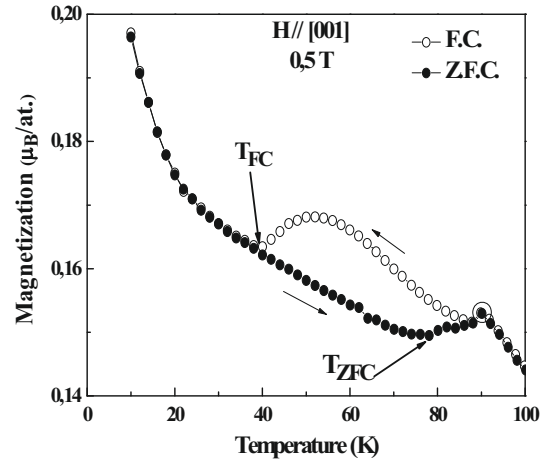


Fig. 5. Thermal variation of the magnetization under a 0.5 T magnetic field applied along the [001] direction for sample F: empty symbols correspond to the FC process (decreasing temperature) and filled ones to the ZFC process (increasing temperature).

bulk, that occur at larger fields, this low field contribution has no influence on the following discussion.

In order to analyze the influence of the field on the temperature of disappearance of D_3 , magnetization measurements have been performed as a function of temperature under a fixed magnetic field. A typical curve is shown for $H = 0.5$ T in Figure 5. This figure exhibits the Field-Cooled (FC) and Zero Field Cooled (ZFC) curves. As in bulk Eu [1], the cusp at 90 K is the signature of the development of helical order. However, at lower temperatures, the thermal variation of the (110) film magnetization is completely different from that of the bulk. In particular: (i) the FC curve exhibits a decrease between 52 K and $T_{FC} = 40$ K; (ii) when increasing temperature after a ZFC process, the magnetization increases at approximately $T_{ZFC} = 77$ K. The FC and ZFC curves are superimposed below 40 K and above 88 K.

These unusual variations of magnetization as a function of temperature can be also correlated to modifications of the proportion of the magnetic domains in agreement with the previous conclusions. The reduction of magnetization during the FC process is attributed to the vanishing of D_3 . Thus, below 40 K, under 0.5 T, D_3 is completely absent. After the ZFC process, the initial magnetic arrangement corresponds to the occurrence of D_1 , with a low susceptibility and the increase of magnetization at 77 K can be attributed to the restoration of D_3 . To summarize, if we compare results obtained for zero field [15], the magnetic field applied along [001] delays the vanishing of D_3 with decreasing temperature and promotes its re-appearance with increasing temperature. This behavior is consistent with the fact that the magnetic field stabilizes the magnetic domain with a propagation vector parallel to the field.

The correlation between the jumps of magnetization and the proportion of D_3 can be explained considering the values of the magnetic susceptibilities of the different domains. Herpin [21] and Nagamiya [22] have calculated

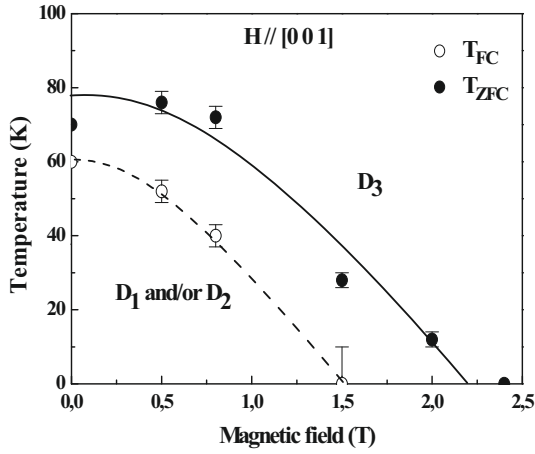


Fig. 6. Magnetic field temperature diagram for film F when the magnetic field is applied along the [001] direction. Empty symbols correspond to T_{FC} the temperature of vanishing of D_3 when decreasing temperature. Filled symbols correspond to T_{ZFC} the temperature of appearance of D_3 when increasing temperature. Continuous lines are guides for the eyes.

the ratio $\chi_{\perp}/\chi_{\parallel}$ in the case of low anisotropy:

$$\frac{\chi_{\perp}}{\chi_{\parallel}} = 2(1 + 2\cos\omega + 2\cos^2\omega) \geq 1$$

χ_{\perp} (χ_{\parallel}) is the susceptibility when the magnetic field is perpendicular (parallel) to the plane of the helix and ω is the turn angle of the helix. The two main hypotheses for this calculation are: (i) when the magnetic field is applied along the helix axis, the turn angle remains unchanged and the magnetic structure is conical; (ii) when the magnetic field is applied in the helix plane, the helix distorts in this plane (the turn angle is modified). This ratio is always larger than 1 and, in the case of bulk Eu, it is close to 6.

In the case of Eu films, the macroscopic magnetization can be expressed as: $M = (P_1\chi_1 + P_2\chi_2 + P_3\chi_3)H$ where χ_i is the magnetic susceptibility associated to D_i . When the magnetic field is applied along [001], $\chi_3 = \chi_{\perp}$ and $\chi_1 = \chi_2 = \chi_{\parallel}$. The magnetic susceptibility of the film is then $\chi = P_3(\chi_{\perp} - \chi_{\parallel}) + \chi_{\parallel}$; it is smaller when $P_3 = 0$ (D_1 and/or D_2 domain configuration and $\chi = \chi_{\parallel}$) than when $P_3 = 1$ (single D_3 domain configuration and $\chi = \chi_{\perp}$). The magnetization data presented in Figure 4c are in agreement with the above conclusions if one consider that, when increasing field, $\chi = \chi_{\parallel}$ when the field is smaller than H_a and $\chi = \chi_{\perp}$ for larger fields.

Finally, a temperature-magnetic field diagram has been constructed from the values of T_{FC} and T_{ZFC} recorded for different applied fields (Fig. 6). When the magnetic field increases, both temperatures decrease. Above the continuous line, only D_3 is present. The field range of occurrence of D_3 grows when increasing temperature. At low field and temperature, only D_1 or D_2 are present. For the values of magnetic field and temperature between both lines, the magnetic arrangement depends on the magnetic history of the sample.

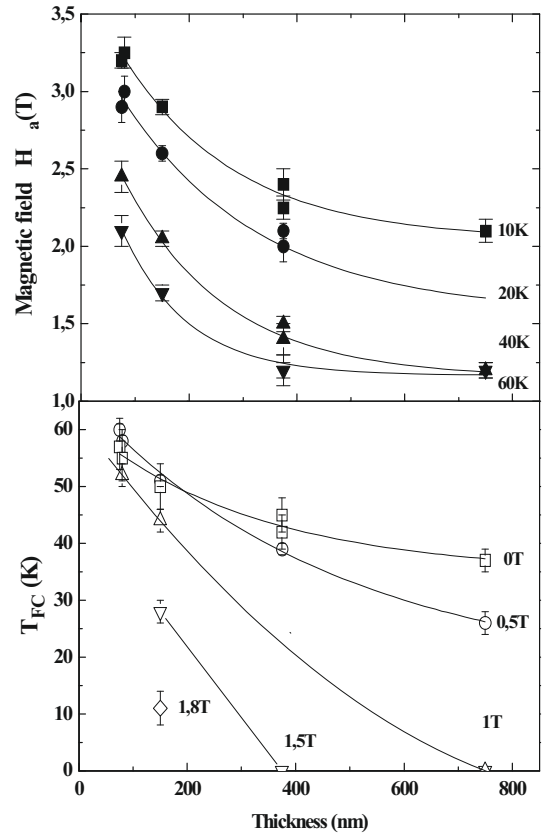


Fig. 7. H_a (a) and T_{FC} (b) as a function of the film thickness for various values of temperature and of the magnetic field. The magnetic field is applied along [001] direction.

The main effect of the magnetic field is to promote D_3 to lower temperatures. This effect is explained by the reduction of $\Delta E(H)$ (the difference between the magnetic energy of D_1 or D_2 and the energy of D_3). Indeed, if $\Delta E(0)$ is the difference between the energy of D_1 or D_2 and the energy of D_3 under zero field: $\Delta E(H) = \Delta E(0) - (\chi_{\perp} - \chi_{\parallel})H^2$. $\Delta E(H)$ is always reduced compared to $\Delta E(0)$ since the Zeeman contribution is negative ($\chi_{\perp} - \chi_{\parallel} > 0$).

3.2.2 Influence of the film thickness

As mentioned in the introduction, the magnetic arrangement under zero magnetic field in (110)Eu films depends on the film thickness. In this section, we describe how the thickness modifies the stability of D_3 in magnetic field.

In particular, Figure 7 shows the variation of H_a (the field of appearance of D_3) and of T_{FC} (the temperature of disappearance of D_3 in a magnetic field) as a function of thickness. Both H_a and T_{FC} increase as film thickness decreases. These growths of H_a and of T_{FC} mean that a stronger field is necessary to obtain D_3 and that D_3 disappears at higher temperature, when the thickness decreases. The range of occurrence of D_3 is thus reduced for the thinnest films.

Table 2. Relative proportions P_i of the magnetic domains at 10 K for samples D, F and G under zero magnetic field. The upper line corresponds to the relative sizes after a zero field cooling, the lower line corresponds to the relative sizes under zero field after applying a magnetic field larger than H_a along the [001] direction.

Sample	P_1 at 10 K (%)	P_2 at 10 K (%)	P_3 at 10 K (%)
Bulk	33.33	33.33	33.33
Film D	0	0	100
Film F	92	8	0
Film G	57	43	0
	12	18	70

Finally, the proportions of the magnetic domains at low temperature were measured in zero field for films D, F and G, after cycling the field. The results are compared with the same proportions after a ZFC process before cycling (Tab. 2). The evolution of proportions of the magnetic domains depends on the film thickness. For the thinnest films (D and F), D_3 is always absent at 10 K whatever the magnetic history is. This result is consistent with the non-zero value of H_d determined from magnetization measurements (Fig. 4c). The effect of field cycling is to reverse the magnetic populations of D_1 and D_2 . On the contrary for the thickest film (film G), D_3 remains populated after switching the field back to zero. However, the behavior of this thick film is still not identical to the bulk one because D_1 and D_2 remain present at 10 K, contrary to the case for bulk Eu (Tab. 2 [13]).

3.3 Magnetic ordering for a magnetic field applied along the $\bar{1}10$ direction

In this section, we report on the results obtained for a magnetic field applied along the in-plane $\bar{1}10$ direction.

a) Neutron diffraction under magnetic field

As in the case for a magnetic field applied along [001], detailed neutron scattering data were obtained as a function of field for the film F. Results for additional samples will be summarized in Section 3.4.

The experiments were performed at 10 K and 65 K after a ZFC process. Since the temperature at which D_3 vanishes is 45 K in film F, the initial magnetic arrangements at zero field are different for 10 K and 65 K: D_3 is absent at 10 K whereas it is still present at 65 K. At both temperatures, D_1 is present and D_2 is absent.

As for a magnetic field applied along the [001] direction: i) the positions of the magnetic satellites do not vary with field which means that neither the turn angle, nor the propagation vectors are modified under field; ii) the intensities vary with magnetic field: they depend on the variation of the proportions of the domains as induced by

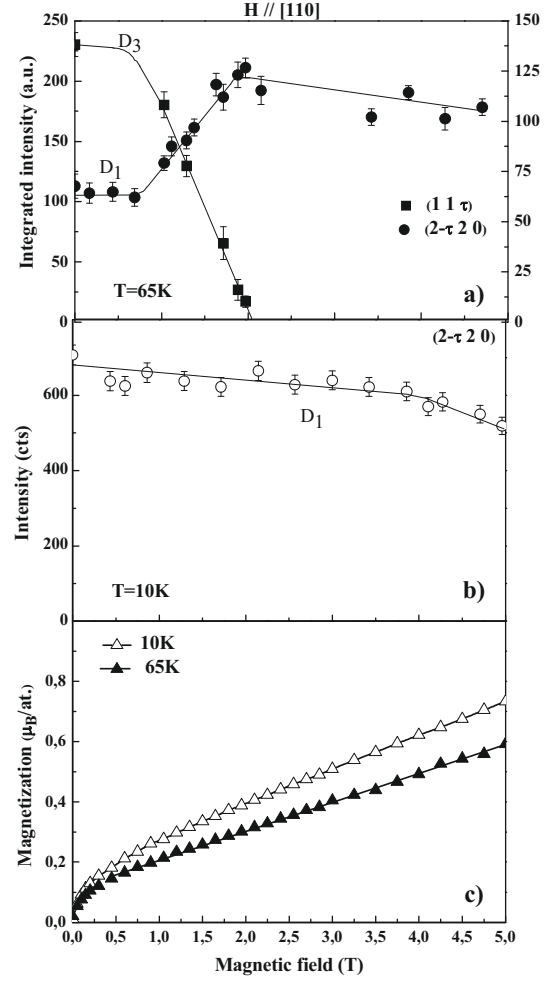


Fig. 8. Intensities of the $(1, 1, \tau)$ and $(2 - \tau, 2, 0)$ magnetic satellites at 65 K (a), intensity of the $(2 - \tau, 2, 0)$ magnetic satellite at 10 K (b) and macroscopic magnetization at 10 K and 65 K (c) as a function of the magnetic field applied along the $\bar{1}10$ direction for sample F. The neutron intensities are collected for increasing magnetic field after a ZFC process.

magnetic field. Figure 8 shows the evolution of the intensity of the $-\kappa_1$ and κ_3 satellites at 65 K (Fig. 8a) and of the $-\kappa_1$ satellite at 10 K (Fig. 8b) with increasing magnetic field.

At 65 K, when the field reaches 0.7 T, the intensity of the $-\kappa_1$ satellite increases whereas the intensity of the κ_3 one decreases (Fig. 8a). This is the signature that D_1 grows at the expense of D_3 . At 2 T, the intensity of the κ_3 satellite and consequently P_3 is zero. The variations of the proportions of the magnetic domain are much less abrupt than in the case of a magnetic field applied along the [001] direction. At 65 K, as in bulk [13], the effect of the magnetic field is to suppress the magnetic domain with wave vector perpendicular to the field (D_3). However, the non-zero value of P_1 is surprising since, in bulk, D_1 and D_2 aren't observed.

At 10 K, the intensity of the $-\kappa_1$ satellite is constant to 3 T and then decreases very slowly with increasing field (Fig. 8b). This result suggests that P_1 is nearly constant.

This is consistent with the fact that this domain is already mainly populated at zero field (97%). The slight decrease of the neutron intensity observed at larger fields could correspond to a distortion of the helix.

For temperatures of 65 K and 10 K, no additional magnetic satellites, corresponding to a magnetic order with a propagation vector parallel to the applied magnetic field, were observed despite intensive search. Contrary to the bulk case, magnetic field applied to the film along $[\bar{1}10]$ favors propagation vectors along a main cube direction as close as possible to H (i.e. along $[100]$).

b) Macroscopic magnetization measurement

At 65 K and 10 K (Fig. 8c), the magnetization curves do not exhibit any jump nor a hysteretic behavior: they are similar to the bulk ones in contrast to the magnetization curves collected for the same film when the field is applied along the $[001]$ direction (Fig. 4c).

Figure 9 presents the thermal variation of the magnetization, after a ZFC and a FC process, for sample F. The magnetic field, applied along $[\bar{1}10]$, is 0.5 T. Similarly to the case where the field is applied along $[001]$: (i) the development of the helical phase give rise to a cusp at 90 K;

(ii) the FC and ZFC curves differ in the temperature range between T_{FC} and T_{ZFC} . However, in this temperature range, the magnetization measured after a ZFC process is *larger* than the magnetization measured after a FC process, in contrast to the result for the field parallel to $[001]$.

We explain the magnetization data considering again the values of the magnetic susceptibilities of the different domains. When the field is applied along $[\bar{1}10]$, the susceptibility for D_3 is now χ_{\parallel} , whereas the susceptibility for D_1 and D_2 is χ_{45° with: $\chi_{45^\circ} = (\chi_{\parallel} + \chi_{\perp})/2$ close to $7\chi_{\parallel}/2$. Thus, the susceptibility of an arrangement with a D_3 domain is smaller than the susceptibility of an arrangement with no D_3 domain.

At 10 K, the absence of a jump on magnetization as a function of field (Fig. 8c) is consistent with the neutron data showing no change of magnetic populations (Fig. 8b).

The $M(H)$ curve measured at 65 K does not exhibit any jump neither, despite the decrease of the D_3 population deduced from neutron measurement. This point is perhaps correlated to the fact that: (i) the values of the susceptibilities χ_{45° and χ_{\parallel} are closer than the ones of χ_{\parallel} and χ_{\perp} are; (ii) the transition is broader.

The larger value of the ZFC magnetization compared to the FC one between T_{ZFC} and T_{FC} (Fig. 9) is in agreement with a smaller susceptibility of D_3 (χ_{\parallel}) compared to the susceptibilities of D_1 and D_2 (χ_{45°). The vanishing of D_3 now generates an increase of susceptibility. In this temperature range, D_3 is present during the FC process and absent during the ZFC one.

3.4 Comparison between $[001]$ and $[\bar{1}10]$ applied field directions

In order to illustrate the different magnetic behavior in (110)Eu films when the magnetic field is applied either

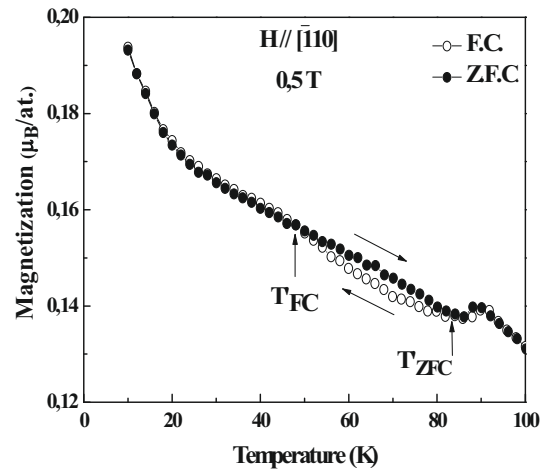


Fig. 9. Thermal variation of the magnetization under a 0.5 T magnetic field applied along the $[\bar{1}10]$ direction for sample F: empty symbols correspond to the FC process and filled ones to the ZFC process.

along the $[001]$ or the $[\bar{1}10]$ direction, Figures 10 and 11 show the variation of T_{FC} (the temperature of disappearance of D_3) as a function of field and of film thickness for both field directions.

In Figure 10, T_{FC} is shown as a function of magnetic field for sample D. For this film, under zero field $T_d = 50$ K (Tab. 1). This figure clearly shows the opposite influence of the $[001]$ and $[\bar{1}10]$ applied fields on the proportion of D_3 . The $[001]$ applied field favors D_3 compared to zero field case. On the contrary, the $[\bar{1}10]$ applied field disfavors this domain.

As it was mentioned previously, $\Delta E(H)$ the difference between the energy of D_3 and the energy of D_1 or D_2 is: $\Delta E(H) = \Delta E(0) - (\chi_3 - \chi_{1or2})H^2$. If the field is parallel to $[001]$, $\chi_3 - \chi_{1or2} = \chi_{\perp} - \chi_{\parallel} > 0$, then the effect of the field is to decrease ΔE . If the field is parallel to $[\bar{1}10]$, $\chi_3 - \chi_{1or2} = \chi_{\perp} - \chi_{45^\circ} < 0$, then the effect of the field is to increase ΔE . The field applied along $[001]$ thus counterbalances the effect due to the lattice strain, i.e. the destabilization of D_3 . On the contrary, the field applied along $[\bar{1}10]$ reinforces the effect due to the lattice strain. Moreover, the field applied along $[001]$ is obviously more effective since $\Delta T_{FC}(H \parallel [001]) > \Delta T_{FC}(H \parallel [\bar{1}10])$. This is likely due to the fact that the $[001]$ direction is a magnetic propagation direction, in other words $|\chi_{\parallel} - \chi_{45^\circ}| < |\chi_{\perp} - \chi_{\parallel}|$.

Figure 11 presents T_{FC} as a function of film thickness with a 0.5 T magnetic field applied along $[001]$ and along $[\bar{1}10]$. The data under zero magnetic field are also presented (T_d). Whatever the value and the direction of the magnetic field are, the temperature at which D_3 vanishes decreases when the film thickness increases. Moreover, this figure illustrates again that: (i) depending on the field direction, the field effect is added or opposed to the lattice strain effect and (ii) the amplitude of this field effect depends on the direction of the applied field (it is larger when the field is applied along $[001]$).

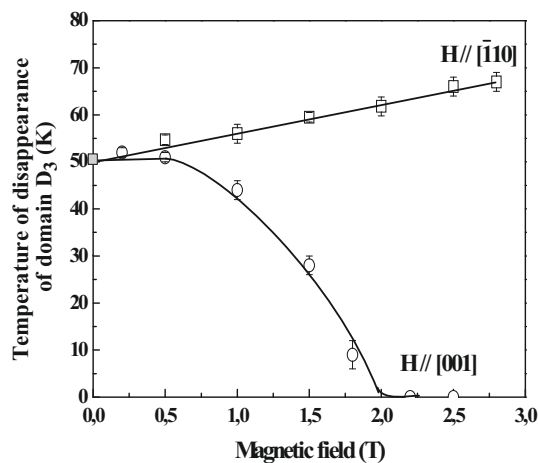


Fig. 10. Temperature of disappearance of D_3 as a function of magnetic field applied along $\bar{1}10$ (squares) and along 001 (circles) for sample F. The value under zero magnetic field is deduced from RXMS experiments.

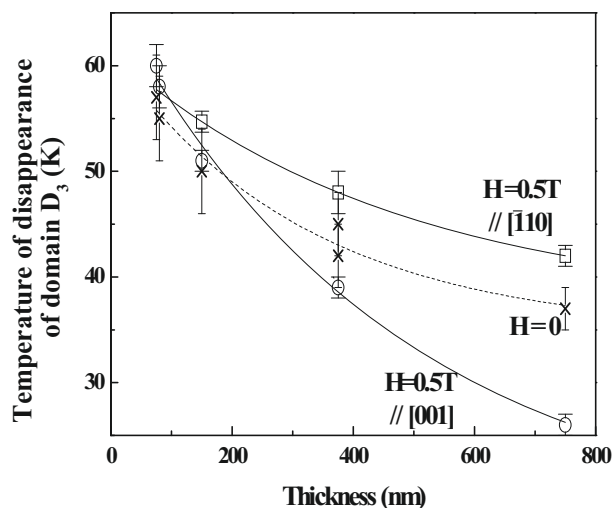


Fig. 11. Temperature of disappearance of D_3 as a function of film thickness when a 0.5 T magnetic field is applied respectively along $\bar{1}10$ (squares) and along 001 (circles) for sample F. The crosses and the dotted line correspond to the temperature of disappearance T_d of D_3 under zero magnetic field when decreasing temperature.

4 Summary and conclusion

In (110)Eu films, at low temperature, the lattice clamping to the substrate induces modifications of the proportions of the magnetic domains and the rotation of propagation vectors of the remaining helices (strain effect). When a magnetic field is applied in the growth plane, the turn angle and the propagation directions of the helices remain unchanged, whereas the proportions of the magnetic domains vary. Actually, compared to the zero field behavior, the Zeeman contribution leads to a reduction of the difference of magnetic energy ΔE between D_1 or D_2 and D_3 when the magnetic field is applied along the 001 direction, on contrast to an increase when the field is parallel

to $\bar{1}10$. Thus, when the field is applied along 001 i.e. along the in-plane magnetic propagation vector, its effect is opposed to the strain effect: it tends to favor D_3 at the expense of the other domains. On the contrary, when the field is applied along the $\bar{1}10$ direction, the effect of the field is added to the strain effect (vanishing of D_3). Moreover, the amplitude of the field effect is larger when the field is along 001 than when the field is along $\bar{1}10$.

Similarly to the lattice strain effect, the effects of the magnetic field depends on the films thickness because the relative contribution of Zeeman energy differs with the relative thickness of the film and the non-magnetic substrate.

Variations of the proportions of the magnetic domains, observed with neutron diffraction experiments explain atypical behavior of the macroscopic magnetization, by considering the different values of the susceptibilities for the different magnetic domains that depend on the angle between the propagation vector of the helices and the applied field.

The experimental results presented in this paper are in agreement with the theory of helical spin ordering and of its modification under magnetic field initially exposed by Nagamiya [22].

Some questions need additional experimental investigations. On one hand, it should be interesting to study the influence of a magnetic field applied along the 100 or the 010 direction at low temperature in a (110)Eu film. Will the Zeeman energy balance the strain effect and align again the propagation vectors along the crystal axes? On another hand, the reason why D_1 is promoted in films and not in bulk when a magnetic field is applied along $\bar{1}10$ needs to be elucidated. Finally, it should be possible to investigate the domain size by spatially resolved magnetic X-ray diffraction [24].

The authors would like to thank the Laboratoire Léon Brillouin (Saclay, France) for providing technical support for neutron diffraction experiments.

References

1. J. Jensen, A.R. Macintosh, *Rare earth magnetism* (Oxford Science Publications, 1991)
2. K. Dumesnil, C. Dufour, P. Mangin, M. Hennion, *Phys. Rev. B* **54**, 6407 (1996)
3. K. Dumesnil, C. Dufour, P. Mangin, M. Hennion, *Europhys. Lett.* **31**, 43 (1995)
4. F. Tsui, C.P. Flynn, *Phys. Rev. Lett.* **71**, 1462 (1993)
5. C. Dufour, K. Dumesnil, A. Mougin, P. Mangin, M. Hennion, *J. Phys.: Cond. Matter* **9**, L131 (1997)
6. J.A. Borchers, M.B. Salamon, R.W. Erwin, J.J. Rhyne, R.R. Du, C.P. Flynn, R.S. Beach, *Phys. Rev. B* **43**, 3123 (1991)
7. C. Dufour, K. Dumesnil, S. Soriano, P. Mangin, P.J. Brown, A. Stunault, N. Bernhoeft, *Phys. Rev. B* **66**, 094428 (2002)
8. P.S. Clegg, J.P. Goff, G.J. McIntyre, R.C.C. Ward, M.R. Wells, *Phys. Rev. B* **67**, 174414 (2003)

9. B.J. Beaudry, P.E. Palmer, J. Less Common Metals **34**, 225 (1974)
10. N.G. Nereson, C.E. Olsen, G.P. Arnold, Phys. Rev. **135**, A176 (1964)
11. R.M. Bozorth, J.H. Van Vleck, Phys. Rev. **118**, 1493 (1960)
12. A.S. Bulatov, O.V. Kovalev, Sov. Phys. Solid State, vol. **30**, 266 (1988)
13. A.H. Milhouse, K.A. McEwen, Solid State Com. **13**, 339 (1973)
14. S. Soriano, K. Dumesnil, C. Dufour, D. Pierre, J. Crystal Growth **265**, 582 (2004)
15. S. Soriano, K. Dumesnil, C. Dufour, T. Gourieux, Ph. Mangin, J.A. Borchers, A. Stunault, Phys. Rev. B **71**, 092409 (2005)
16. S. Soriano, C. Dufour, K. Dumesnil, J.A. Borchers, Ph. Mangin, Appl. Phys. Lett. **85**, 4636 (2004)
17. K.A. McEwen, G.J. Cock, L.W. Roeland, A.R. Mackintosh, Phys. Rev. Lett. **30**, 287 (1973)
18. C. Sürgers, M. Schöck, H.V. Löhneysen, Surf. Sci. **471**, 209 (2001)
19. A. Mougin, C. Dufour, K. Dumesnil, N. Maloufi, Ph. Mangin, G. Patrat, Phys. Rev. B **59**, 5950 (1999)
20. H. Zabel, J. Phys. Cond. Matter. **11**, 9303 (1999)
21. A. Herpin, *Théorie du magnétisme* (INSTN-PUF, 1968)
22. T. Nagamiya, K. Nakata, Y. Kitano, Prog. Theor. Phys. (Kyoto) **27**, 1253 (1962)
23. A.E. Clark, *Handbook on the physics and chemistry of rare earths*, edited by, K.A. Gschneider Jr, L. Eyring (North Holland Publishing, 1979), Vol. 2, Chap. 15
24. P.G. Evans, E.D. Isaacs, J. Phys. D: Appl. Phys. **39** (2006) R245